RSC Advances

PAPER

View Article Online
View Journal | View Issue

Cite this: *RSC Adv.*, 2018, **8**, 32317

Group-IVA element-doped $SrIn_2O_4$ as potential materials for hydrogen production from water splitting with solar energy

Hai-Cai Huang,[a] Chuan-Lu Yang, *[a] Mei-Shan Wang,[a] Xiao-Guang Ma[a] and You-Gen Yi[b]

Band gap engineering can efficiently improve the photocatalytic activity of semiconductors for hydrogen generation from water splitting. Herein, we present a comprehensive investigation on the geometrical structures, electronic, optical, and potential photocatalytic properties and charge carrier mobility of pristine and group-IVA element-doped $SrIn_2O_4$ using first-principles density functional theory with the meta-GGA+MBJ potential. The calculated formation energies are moderate, indicating that the synthesis of the doped structures is experimentally feasible. In addition, the energy band gaps of the group-IVA element-doped $SrIn_2O_4$ range from 1.67 to 3.07 eV, which satisfy the requirements for photocatalytic water splitting, except for that of the Si mono-doped structure. Based on the deformation potential theory, a high charge carrier mobility of 2093 $cm^2\ V^{-1}\ s^{-1}$ is obtained for the pristine $SrIn_2O_4$ and those of the doped-structures are also large, although a decrease in the values of some are observed. The optical absorption coefficient of the doped structures in the near ultraviolet (UV) and visible light range significantly increases. Therefore, group-IVA element-doped $SrIn_2O_4$ are potential candidates as photocatalysts for hydrogen generation from water splitting driven by visible light.

Received 29th May 2018
Accepted 4th September 2018

DOI: 10.1039/c8ra04569k

rsc.li/rsc-advances

1. Introduction

Hydrogen is considered as one of the future fuels, and thus has attracted increasing attention as renewable and clean energy.[1–4] The conversion of solar energy into hydrogen by a photocatalyst *via* water splitting is an attractive technology, which can efficiently reduce the severe environment and energy issues.[5–7] Photocatalytic water splitting is regarded as artificial photosynthesis, which involves three main steps: (i) absorption of photons with equivalent or greater energy than the band gap of the semiconductor photocatalyst, where electrons are excited from the valence band to the conduction band, leading to the generation of electron–hole pairs. (ii) The photoexcited carriers migrate to the surface of the photocatalyst. (iii) The separated photoexcited carriers reduce H^+ to produce H_2 and oxidize H_2O to produce O_2.[8] Generally, only water, solar energy, and photocatalyst are needed for photocatalytic water splitting, where solar energy is inexhaustible and water is one of the most abundant resources on earth. Therefore, the key factor to achieve efficient photocatalytic water splitting is the development of suitable photocatalysts. Since the photocatalytic production of hydrogen from water splitting by TiO_2 was reported in 1972,[9] much effort has been dedicated to improving the hydrogen production efficiency.[10] In recent years, the integration of atomic dopants has been confirmed to be an important approach for improving the efficiency of photocatalytic water splitting.[11] Doping can efficiently enhance the photocatalytic performance by extending the absorption edge of semiconductors to a lower energy range. For example, Mg-doped anatase TiO_2 had been synthesized successfully by Gao et *al.*[12] They found that the absorption coefficient of TiO_2 increased with an increase in the Mg doping concentration. Highly efficient photocatalytic water splitting was achieved on Pt-embellished 0.5% Mg–TiO_2, and the hydrogen evolution reached as high as 850 μmol g^{-1} h^{-1}. Also, metal ion (Nb, Cr, Cu, and Ni) and nitrogen (N) co-doped TiO_2 photocatalysts were synthesized by Lin *et al.*,[13] and they found that the significant photocatalytic enhancement of the Cu, N co-doped TiO_2 was attributed to the enhanced visible light absorption. Similarly, Cu-doped ZnS microspheres were prepared *via* microwave hydrothermal method by Lee *et al.*[14] They reported that the absorption coefficient of ZnS in the visible light range was significantly enhanced with the introduction of Cu dopant, and the hydrogen evolution rate reached as high as 973.1 μmol g^{-1} h^{-1} under ZnS with 2 mol% Cu dopant.

Two groups of elements can act as active components in photocatalytic water splitting.[15] Photocatalysts with a d^0 or d^{10} electronic configuration generally present a better photo-

[a]*School of Physics and Optoelectronics Engineering, Ludong University, Yantai 26425, People's Republic of China. E-mail: ycl@ldu.edu.cn; Tel: +86 535 6672870*

[b]*Hunan Key Laboratory for High-Microstructure and Ultrafast Process, College of Physics and Electronics, Central South University, Changsha 410083, People's Republic of China*

response than that with partially filled d orbitals. As one of the p-block metal oxides with a d^{10} electronic configuration, $SrIn_2O_4$ has been reported to exhibit stable and high photocatalytic activity for water splitting.[16] However, its energy band gap is 3.6 eV,[17] indicating that it only responds to ultraviolet (UV) light, which is only about 7% of solar energy.[18] Therefore, $SrIn_2O_4$ photocatalytic water splitting cannot efficiently utilize solar energy. Also, its rate of hydrogen formation is only about 7 μmol g^{-1} h^{-1}, which is much smaller than that of TiO_2 (106 μmol g^{-1} h^{-1}).[19,20] Considering that band gap engineering is an effective method to extend the absorption edge of photocatalysts to the visible light range, there are several reports on cation/anion doped $SrIn_2O_4$ to efficiently use solar energy.[21–24] For example, Dy^{3+}/Pr^{3+}/Tb^{3+}-doped $SrIn_2O_4$ was successfully prepared by Liu *et al.*[25] They found that $SrIn_2O_4$:Dy^{3+}/Pr^{3+}/Tb^{3+} exhibited stronger near white, red and green luminescence, which results from the efficient energy transfer from the host lattice to the dopants. Additionally, Eu^{3+}, Sm^{3+}-doped $SrIn_2O_4$ was successfully synthesized by Li *et al.*[26] through a combustion method. They found that Sm^{3+}-doped $SrIn_2O_4$ effectively extended and strengthened the absorption range from 400 to 405 nm.

However, to the best of our knowledge, there are no experimental or theoretical investigations on group-IVA element-doped $SrIn_2O_4$. Therefore, we comprehensively investigate the electronic, optical, and potential photocatalytic properties and carrier mobility (μ) for pristine and IVA-doped $SrIn_2O_4$ to understand the influence of the dopants on the photocatalytic properties of $SrIn_2O_4$ for water splitting. A high μ is observed for the pristine $SrIn_2O_4$, which implies that the carriers can transfer to its surface efficiently in the process of photocatalytic water splitting. The absorption coefficient of $SrIn_2O_4$ in the visible light range is significantly enhanced with the introduction of the dopants, and the mechanism is explored in accordance with the total density of states (TDOS) and partial density of states (PDOS). The results obtained are beneficial for the design of new photocatalytic materials driven by visible light.

2. Computational details

In this study, a 2 × 2 × 2 supercell of $SrIn_2O_4$ with the space group *Pnam* belonging to orthorhombic symmetry, containing 8 Sr atoms, 16 In atoms and 32 O atoms, was constructed. The IVA-doped structures were built by substituting the Sr atom with IVA atoms, which correspond to a doping molar concentration of 1.5%. Hereafter, the doped structures are denoted as C@Sr, Si@Sr, Ge@Sr, Sn@Sr, and Pb@Sr. In the present study, all the density functional theory (DFT) simulations were carried out using the Vienna Ab initio simulation package (VASP).[27] The projector augmented wave (PAW) potential[28] was used to describe the ion–electron interactions, which means that $2s^22p^4$ for O, $4d^{10}5s^2$ for Sr, $5s^25p^1$ for In, $2s^22p^2$ for C, $3s^23p^2$ for Si, $4s^24p^2$ for Ge, $5s^25p^2$ for Sn and $6s^26p^2$ for Pb were treated as valence electrons. The electron exchange-correlation functional was treated as the generalized gradient approximation (GGA) with the Perdew–Burke–Ernzerhof (PBE) parametrization for structural optimization.[29] All the atomic positions were fully relaxed until the residual forces and energy convergence were less than 0.01 eV $Å^{-1}$ and 10^{-6} eV, respectively. The plane-wave cutoff kinetic energy was set as 450 eV throughout the calculation. For the geometry optimization and electronic properties calculation, Monkhorst–Pack *k*-point grids of 3 × 3 × 5 and 5 × 5 × 7 were used. The meta-GGA+MBJ potential[30] was used to obtain credible calculations for the energy gap and optical absorption coefficient.

To confirm the validity of the present calculational results, we performed additional calculations for $CaIn_2O_4$/GaN/GaAs/ZnS and C/Pb-doped ZnS, which were synthesized experimentally. For the pristine structures, we investigated the geometrical structures and energy band gaps of $CaIn_2O_4$, GaN, and GaAs, as listed in Table 1. The results from Table 1 show that the lattice parameters of $CaIn_2O_4$ are $a = 9.735$, $b = 11.389$ and $c = 3.249$ Å, which are slightly larger than the experimental values.[31] The calculated energy band gap of $CaIn_2O_4$ is 3.67 eV, which is also close to the experimental value[31] and that of GaN and GaAs,[32–35] indicating that the present theoretical level is rational for the pristine structure. For the doped structure, we investigated the energy band gap of C, Pb-doped ZnS. The results from Table 2 show that the parameters and energy band gaps of the pristine ZnS are almost close to that obtained in the previous works,[36,37] whereas, the calculated energy band gaps of C, Pb-doped ZnS are 0.3 eV smaller than the experimental value.[38,39] However, it is still acceptable for us. In addition, the carrier mobility of GaAs was also investigated. The results in Table 3 demostrate that the calculated carrier mobility of the pristine GaAs is 0.594 m^2 V^{-1} s^{-1}, which is in good agreement with the experimental values.[40] All of these results indicate that the present theoretical level is rational and that the results for $SrIn_2O_4$ herein are credible.

Table 1 Calculated lattice parameters *a*, *b*, and *c* (Å), and energy band gaps, E_g (eV), for the experimentally synthesized semiconductors

	Lattice parameter			
	a	*b*	*c*	E_g
$CaIn_2O_4$	9.735	11.389	3.249	3.67 eV
	9.720 (ref. 31)	11.300 (ref. 31)	3.240 (ref. 31)	3.90 eV (ref. 31)
GaN	3.219	3.219	5.230	3.32 eV
	3.189 (ref. 32)	3.189 (ref. 32)	5.185 (ref. 32)	3.40 eV (ref. 33)
GaAs	5.726	5.726	5.726	1.45 eV
	5.653 (ref. 34)	5.653 (ref. 34)	5.653 (ref. 34)	1.44 eV (ref. 35)

Table 2 Calculated lattice parameters *a*, *b*, and *c* (Å), and energy band gaps, E_g (eV), for the pristine and C/Pb doped ZnS

	$a = b = c$	E_g
Pristine	5.436	3.57 eV
	5.412 (ref. 36)	3.70 eV (ref. 37)
C@ZnS	5.422	2.25 eV
	—	1.95 eV (ref. 38)
Pb@ZnS	5.480	2.59 eV
	—	2.30 eV (ref. 39)

Table 3 Calculated carrier mobility, μ ($m^2\ V^{-1}\ s^{-1}$), for GaAs

	Type	C_β	E_β	m^*_{dos}	μ
Pristine	Electron	0.65	16.68	0.11	0.594
		—	—	—	0.700 (ref. 40)

3. Results and discussion

3.1 Geometrical structures and energy stability of $SrIn_2O_4$

The optimized structure of Sn@Sr in Fig. 1 is used to represent the IVA-doped $SrIn_2O_4$ structures and the others are omitted for brevity. The optimized lattice parameters of the pristine and doped $SrIn_2O_4$ are presented in Table 4. The calculated lattice parameters of the pristine $SrIn_2O_4$ are $a = 9.906$, $b = 11.602$ and $c = 3.305$ Å, which are in great agreement with the previous works.[26,41] For the doped structures, all the changes in the lattice parameters are less than 0.1 Å compared to that of the pristine structure, which means that the dopants did not lead to significant deformation of the lattice.

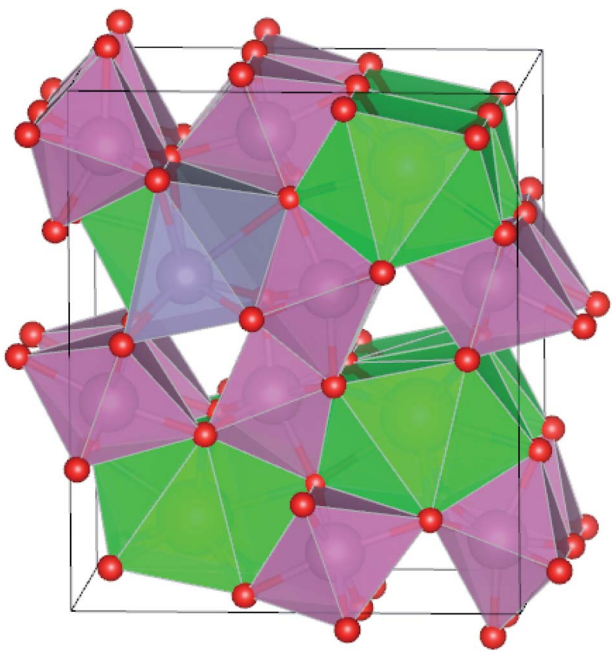

Fig. 1 Optimized structure of Sn@Sr. The green, purple, red and gray spheres represent the Sr, In, O, and Sn elements, respectively.

To evaluate the feasibility of the synthesis of the doped $SrIn_2O_4$, the formation energy (E_{form}) was calculated as follows:[42]

$$E_{form} = E(\text{doped}) - E(\text{pristine}) - n\mu_X + n\mu_{Sr} \quad (1)$$

where, E(doped) and E(pristine) are the total energy of the doped and pristine $SrIn_2O_4$, respectively. μ_X and μ_{Sr} represent the chemical potential of the dopants and Sr atom, respectively. The calculated E_{form} of the doped structures are collected in Table 4. The results demonstrate that the E_{form} of the doped structures are in the range of 4.40 to 6.74 eV, which is acceptable for their general synthesis.

3.2 Photocatalytic water splitting and band engineering

The calculated energy band gaps (E_g) of all the structures are listed in Table 4. The E_g of 3.61 eV for the pristine $SrIn_2O_4$ is close to the experimental value,[17] which signifies that the present theoretical level is credible. However, it is too large to respond to visible light. Thus, band gap engineering of the electronic properties of $SrIn_2O_4$ is necessary. Fortunately, the results in Table 4 demonstrate that the E_g of $SrIn_2O_4$ significantly decreased with the introduction of IVA elements, especially for C@Sr and Si@Sr. However, one can find from Table 4 that the change tendency of the energy band gaps for the doped structures is not singlet, which is similar to the case of IVA-doped ZnS.[43] The change tendency of the ionization energy of IVA elements is responsible for the characteristic of the energy band gaps. For examples, the ionization energy of Si is smallest and that of Pb is the largest, which results in the smallest E_g of Si@Sr and the largest E_g of Pb@Sr among the doped structures, respectively. The E_gs of the doped structures are in the range from 1.32 eV to 3.07 eV, implied that all the doped structures can respond to the visible light. The E_g for photocatalytic water splitting should be higher than 1.23 eV considering the minimum potential for water splitting is 1.23 eV, while an E_g smaller than 3.0 eV means that the photocatalytic water splitting reaction can be efficiently driven by visible light.[44] Moreover, the suitable band edge position of a semiconductor is also indispensable for photocatalytic water splitting. The valence band maximum (VBM) of a photocatalyst must be lower than the oxidation potential ($V_{O2/H2O} = -5.67$ eV) so that it can be used for oxygen production, while its conduction band minimum (CBM) must be higher than the reduction potential ($V_{H2/H^+} = -4.44$ eV) for hydrogen production.[45] The VBMs and CBMs of the present structures can be calculated from the following equations:[46]

$$E_{VBM} = -\chi - \frac{1}{2}E_g \quad (2)$$

$$E_{CBM} = -\chi + \frac{1}{2}E_g \quad (3)$$

where, χ is the Mulliken electronegativity value of the compound and E_g is the energy band gap of the structure. The electronegativity can be determined using the following equation:[47]

Table 4 Calculated lattice parameters *a*, *b*, and *c* (Å), energy band gaps E_g (eV), formation energies E_{form} (eV) and electronegativity χ (eV) for $SrIn_2O_4$

	Lattice parameters					
	a	*b*	*c*	E_g	E_{form}	χ
Pristine	9.906	11.602	3.305	3.61 eV	—	4.84
	9.830 (ref. 24)	11.496 (ref. 24)	3.269 (ref. 24)	3.60 eV (ref. 17)		
	9.809 (ref. 29)	11.449 (ref. 29)	3.265 (ref. 29)			
C@Sr	10.006	11.578	3.306	1.67 eV	4.92	4.94
Si@Sr	9.994	11.586	3.303	1.32 eV	4.40	4.91
Ge@Sr	9.954	11.586	3.297	2.64 eV	6.14	4.91
Sn@Sr	9.926	11.616	3.302	2.31 eV	6.62	4.91
Pb@Sr	9.920	11.620	3.305	3.07 eV	6.74	4.90

$$\chi = -\left(\frac{\partial E}{\partial N}\right)_v = [E(N+1) - E(N) + E(N) - E(N-1)]/2 \approx (I + A)/2 \quad (4)$$

where, I is the ionization energy and A is the electron affinity of the atom. Using eqn (4), the electronegativities of Sr, In, O, C, Si, Ge, Sn, and Pb were calculated. The Mulliken electronegativity of a compound can be considered as the electronegativity of its constituent atoms, which corresponds to the following equation:[48]

$$\chi(\text{compound}) = \chi_1^a \chi_2^b \ldots \chi_n^c \quad (5)$$

where, χ_1, χ_2 and χ_n represent the electronegativities of the atoms in the compound, and a, b, and c are the molar fractions of the atoms. The electronegativities of the pristine and doped $SrIn_2O_4$ were calculated based on eqn (5), and the results are listed in Table 4. The results reveal that the electronegativities of the doped structures are larger than that of the pristine structure, which can be understood from the fact that the electronegativities of IVA elements are larger than that of the Sr atom. As a result, the reductive ability of the doped structures is stronger than that of the pristine structure. Base on eqn (2)–(5), the calculated absolute CBMs and VBMs of the pristine and doped $SrIn_2O_4$ are shown in Fig. 2. This figure shows that the CBM of the pristine $SrIn_2O_4$ is −3.04 eV, which is more positive than the reduction potential V_{H2/H^+}, and the VBM is more negative than the oxidation potential $V_{O2/H2O}$, indicating that it can be used for hydrogen production from water splitting. It can also be observed that the CBMs and VBMs of the IVA-doped structures shift toward the potential of the water oxidation and reduction reactions in Fig. 2. Fortunately, all the CBMs and VBMs except that of Si@Sr satisfy the requirements for the water splitting reaction. Therefore, the pristine $SrIn_2O_4$ and the C@Sr, Ge@Sr, Sn@Sr and Pb@Sr structures are favorable for photocatalytic water splitting.

3.3 Enhancement of absorption coefficient of IVA-doped $SrIn_2O_4$

Enhancement of the absorption coefficient of $SrIn_2O_4$ in the visible light range can promote the full use of solar energy to produce hydrogen from photocatalytic water splitting. Thus, to evaluate the absorption coefficient of $SrIn_2O_4$, its complex dielectric function was first calculated. The details of the calculation of the complex dielectric function can be found in the previous literature[49] and is thus omitted here for brevity. The results are plotted in Fig. 3, which shows that the imaginary

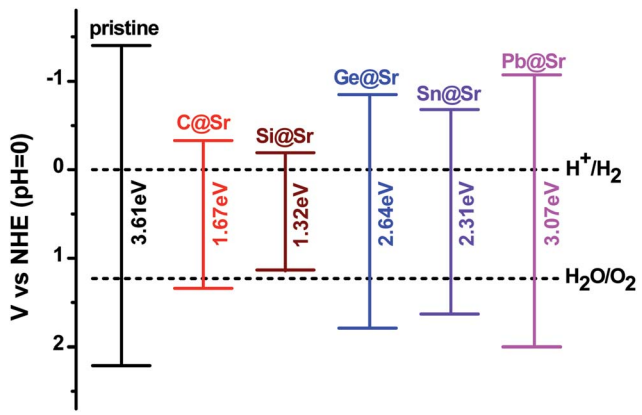

Fig. 2 Absolute VBM and CBM energy levels relative to the NHE potential for the pristine and doped $SrIn_2O_4$.

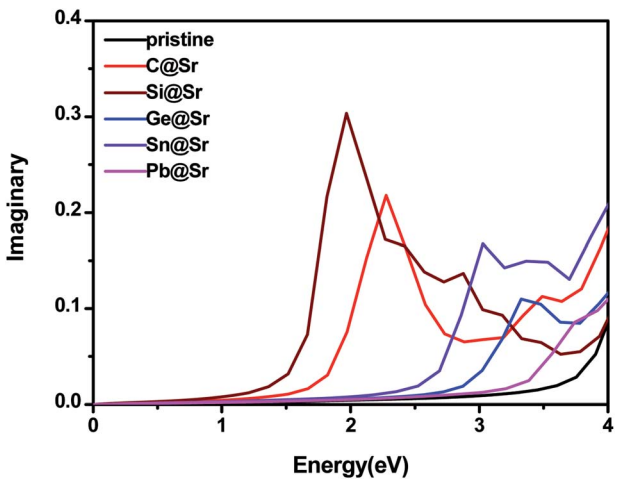

Fig. 3 Imaginary part of the dielectric function of the pristine and doped $SrIn_2O_4$.

part $\varepsilon_2(\omega)$ of the dielectric function of the pristine $SrIn_2O_4$ is close to zero in the visible and infrared light range. Nevertheless, a significant red-shift of $\varepsilon_2(\omega)$ was observed when $SrIn_2O_4$ is doped with IVA elements, especially for C@Sr and Si@Sr.

The optical absorption properties can be deduced from the complex dielectric function according to the following expression:[50]

$$\alpha(\omega) = 2\omega\left(\frac{\left[{\varepsilon_1}^2(\omega) + {\varepsilon_2}^2(\omega)\right]^{\frac{1}{2}} - \varepsilon_1(\omega)}{2}\right)^{\frac{1}{2}} \quad (6)$$

where, α is the optical absorption coefficient. Fig. 4 shows the absorption coefficient of the pristine and doped $SrIn_2O_4$. The results reveal that the pristine $SrIn_2O_4$ shows no significant absorption in the visible light range, which is in agreement with the previous works.[51] Therefore, the pristine $SrIn_2O_4$ does not respond to visible light, and as a result, its photocatalytic efficiency using solar energy is low. Nevertheless, significant red-shifts due to absorption are identified for the IVA-doped structures, especially for C@Sr, Si@Sr, and Ge@Sr, where a significant enhancement in absorption in the visible light range is observed. This indicates that these structures are preferable to the pristine structure to capture solar energy in the photocatalytic water splitting reaction.

3.4 Density of states and partial density of states

To understand the origin of the visible light absorption of the IVA-doped structures, their TDOS and PDOS were calculated, as shown in Fig. 5 and 6, respectively. Fig. 5 shows new energy levels resulting from the doped IVA elements in the band gap of the pristine structure, which are responsible for the reduction in the energy band gap of the doped structures. The effect of the dopants on PDOS of $SrIn_2O_4$ is demonstrated in Fig. 6. Fig. 6a shows that VBM of the pristine $SrIn_2O_4$ is mainly dominated by O 2p states with a small number of 4p, 4d and 5s states of Sr as well as 4d states of In, while its CBM is mainly dominated by 5s states of In with a small number of 5s states of Sr, as well as 2s and 2p states of O. However, a new additional donor energy level mainly comprising of p states from the dopant is observed in the band gap of $SrIn_2O_4$ after the IVA doping. Specifically, the electron transfer from the p states of the dopants to the 5s states of In is responsible for the significant enhancement in the absorption of the doped $SrIn_2O_4$ in the visible light range. Moreover, the energy of the CBM for the doped structures remained unchanged although the components are changed compared to that of the pristine structure.

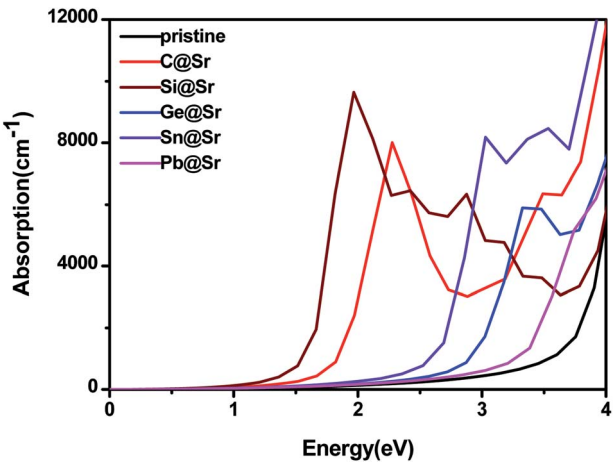

Fig. 4 Absorption coefficient of the pristine and doped $SrIn_2O_4$.

3.5 Effective mass and carrier mobility

The efficient separation of charge carriers and high mobility μ significantly impact the efficiency of photocatalytic water splitting. Thus, μ and relative ratio (D) between the effective mass of electrons (m_e^*) and holes (m_h^*) for the pristine and doped $SrIn_2O_4$ were calculated considering the relaxation time (τ) as follows:[52]

$$\mu = \frac{q\tau}{m^*} \quad (7)$$

where, q is the carrier charge and m^* is the effective mass of the charge carriers. τ can be calculated depending on the detailed scattering mechanisms. For a three-dimensional system, τ along the β-direction at temperature T can be expressed as follows:[53]

$$\tau_\beta = \frac{2\sqrt{2\pi}C_\beta\hbar^4}{3\left(k_B T m_{dos}^*\right)^{2/3}{E_\beta}^2} \quad (8)$$

where, ħ represents the reduced Planck constant and k_B stands for the Boltzmann constant. C_β is the elastic constant, which can be calculated as $C_\beta = \frac{1}{V_0}\frac{\partial^2 E}{\partial(\Delta l/l_0)^2}|_{l=l_0}$, where, E is the total energy of the structure, l_0 is the lattice constant along the β-direction, $\Delta l = l - l_0$ is the corresponding lattice distortion, and V_0 is the equilibrium volume of the unit cell. The deformation potential constant E_β is calculated by $E_\beta = \frac{\partial E_{edge}}{\partial(\Delta l)/l_0}$, where, E_{edge} is the energy level of the electrons in the CBM and holes in the VBM. The density-of-states effective mass m_{dos}^* is given by $m_{dos}^* = \hbar^2\left(\frac{d^2E_{edge}}{dk^2}\right)^{-1}$. The calculated C_βs, E_βs, m_{dos}^* and μs of the pristine and doped $SrIn_2O_4$ are summarized in Table 5. A larger μ represents a higher migration rate of photogenerated charge carriers, which leads to charge carriers quickly reaching the surface of the materials to drive the redox reaction for hydrogen and oxygen production. The results in Table 5 reveal that the calculated μ of the electrons in the pristine $SrIn_2O_4$ is 2093.00 $cm^2\ V^{-1}\ s^{-1}$, while that of the holes is only about 0.97 $cm^2\ V^{-1}\ s^{-1}$, indicating that the separation of electrons and the holes is significant. Therefore, the pristine $SrIn_2O_4$ is beneficial for water splitting. Moreover, the μ of the electrons in the doped structures is higher than that of other effective photocatalytic materials, such as MoS_2 (200 $cm^2\ V^{-1}\ s^{-1}$),[54] although it significantly decreases compared with that of the pristine structure. As a result, IVA-doped $SrIn_2O_4$ also exhibits efficient photocatalytic behavior theoretically.

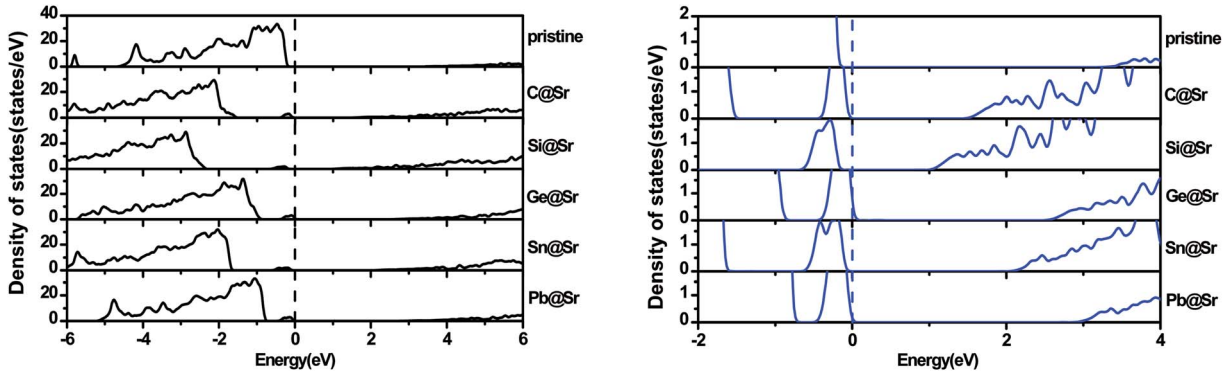

Fig. 5 Total density of states for the pristine and doped $SrIn_2O_4$.

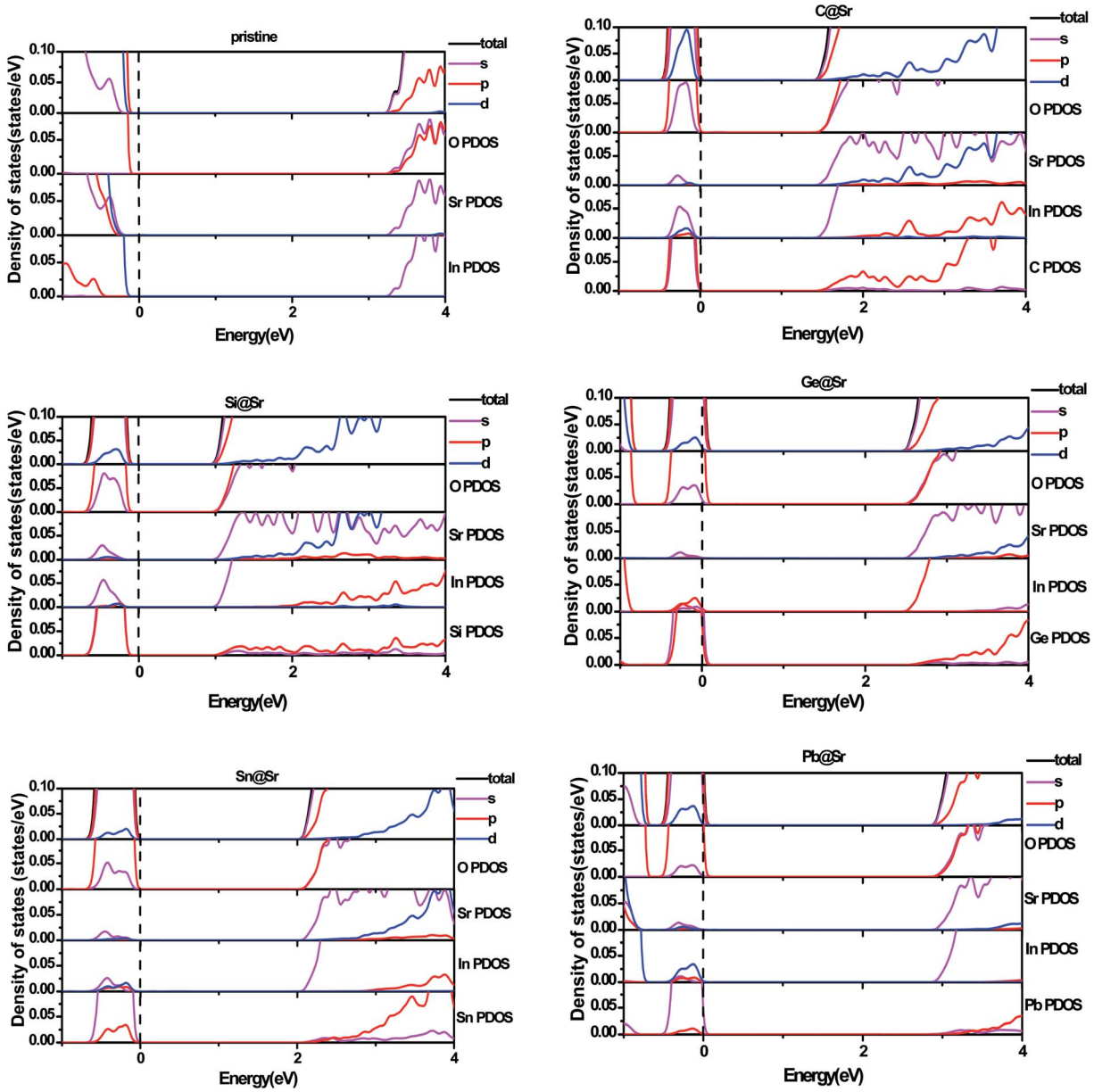

Fig. 6 Partial density of states for pristine and doped $SrIn_2O_4$.

Table 5 Calculated elastic constant C_β (N m^{-1}), deformation potential constant E_β (eV), density-of-states effective mass m^*_{dos}, relaxation time τ (fs) and carrier mobility μ (cm^2 V^{-1} s^{-1}) for $SrIn_2O_4$

	Type	C_β	E_β	m^*_{dos}	μ	D
Pristine	Electron	1.55	16.15	0.24	2093.00	27.83
	Hole		11.61	6.68	0.97	
C@Sr	Electron	1.53	14.80	0.59	250.98	19.34
	Hole		13.08	11.41	0.20	
Si@Sr	Electron	1.51	15.56	0.90	79.37	8.16
	Hole		13.82	7.34	0.53	
Ge@Sr	Electron	1.54	16.12	0.29	1214.70	17.28
	Hole		13.19	5.01	1.54	
Sn@Sr	Electron	1.52	16.49	0.47	353.02	5.68
	Hole		14.11	2.67	6.43	
Pb@Sr	Electron	1.53	16.35	0.37	674.00	7.62
	Hole		13.17	2.82	6.49	

The recombination of electrons and holes is one of the factors that limits the photoactivity of a semiconductor. Thus, to further analyze the recombination rate of electrons and holes, the relative ratio (D) between the effective mass of electrons (m^*_e) and holes (m^*_h) was calculated according to the following expression:[55]

$$D = \frac{m^*_h}{m^*_e}$$

A high value of D is related to a great distinction between the mobility of electrons and holes, which reduces the probability of their recombination. The absolute D values of the pristine and doped $SrIn_2O_4$ are listed in Table 5. Evidently, the D value of 27.83 for the pristine $SrIn_2O_4$ implies the efficient separation of photogenerated charge carriers. The D values of the doped structures show a slight decrease; however, they are still several times higher than that of many typical photocatalytic materials, such as TiO_2 (0.97),[56] $BiVO_4$ (1.42),[57] and WS_2 (1.36).[57] Therefore, both the pristine and IVA-doped $SrIn_2O_4$ are efficient photocatalysts with satisfactory photogenerated charge carrier recombination rates.

4. Conclusion

The feasibility and properties of IVA-doped $SrIn_2O_4$ as photocatalysts for hydrogen production from water splitting were investigated. The geometrical, electronic and optical properties and carrier mobilities of all the considered structures were calculated using first-principles DFT with the meta-GGA+MBJ potential. The energy levels of the CBM and VBM for all the structures except for Si@Sr satisfy the requirements of photocatalytic water splitting, although the E_g of the doped structures decreased by 1.94, 2.29, 0.97, 1.30 and 0.54 eV in comparison with that of the pristine structure. Moreover, the absorption coefficients in the visible light range are significantly enhanced, especially for the C@Sr, Si@Sr and Ge@Sr structures, which indicates that the photocatalytic water splitting by C@Sr and Ge@Sr can be efficiently driven by solar energy. The TDOS and PDOS of these structures demonstrate that the new additional donor energy levels mainly comprising of the p states of the dopants are responsible for the reduction in energy band gap and enhancement of absorption coefficient in the visible light range. In addition, a high carrier mobility and efficient separation of photogenerated charge carriers are observed for both the pristine and doped structures, which lead to efficient photocatalytic performances. Therefore, we predict that C@Sr and Ge@Sr are the most promising candidates as photocatalysts for hydrogen production from water splitting driven by visible light.

Conflicts of interest

There are no conflicts of interest to declare.

Acknowledgements

This study was supported by the National Natural Science Foundation of China (NSFC) under Grant Nos. NSFC-11374132 and NSFC-11574125, as well as the Taishan Scholars Project of Shandong Province (ts201511055).

References

1 F. J. López-Tenlladoa, J. Hidalgo-Carrilloa, V. Montesa, A. Marinasa, F. J. Urbanoa, J. M. Marinasa, L. Ilievab, T. Tabakovab and F. Reida, *Catal. Today*, 2017, **280**, 58–64.
2 K. N. Li, C. L. Yang, Y. X. Han, M. S. Wang and L. Z. Wang, *Energy*, 2016, **106**, 131–136.
3 B. C. Qiu, Q. H. Zhu, M. M. Du, L. G. Fan, M. Y. Xing and J. L. Zhang, *Angew. Chem.*, 2017, **129**, 2728–2732.
4 H. C. Huang, C. L. Yang, M. S. Wang and X. G. Ma, *Int. J. Hydrog. Energy*, 2017, **42**, 15464–15470.
5 B. H. Wu, D. Y. Liu, S. Mubeen, T. T. Chuong, M. Moskovits and G. D. Stucky, *J. Am. Chem. Soc.*, 2016, **138**, 1114–1117.
6 Z. K. He, J. W. Fu, B. Cheng, J. G. Yu and S. W. Cao, *Appl. Catal. B.*, 2017, **205**, 104–111.
7 A. Carrero, A. J. Vizcaíno, J. A. Calles and L. García-Moreno, *J. Energy Chem.*, 2017, **26**, 42–48.
8 K. Maeda, *J. Photochem. Photobiol., C*, 2011, **12**, 237–268.
9 A. Fujishima and K. Honda, *Nature*, 1972, **238**, 37–38.
10 K. Maeda and K. Domen, *J. Phys. Chem. Lett.*, 2010, **1**, 2655–2661.
11 B. C. Zhu, J. F. Zhang, C. J. Jiang, B. Cheng and J. G. Yu, *Appl. Catal. B.*, 2017, **207**, 27–34.
12 L. J. Gao, Y. G. Li, J. B. Ren, S. F. Wang, R. N. Wang, G. S. Fu and Y. Hu, *Appl. Catal. B.*, 2017, **202**, 127–133.
13 H. Lin and C. Shih, *J. Mol. Catal. A: Chem.*, 2016, **411**, 128–137.
14 G. J. Lee, S. Anandan, S. J. Masten and J. J. Wu, *Renewable Energy*, 2016, **89**, 18–26.
15 K. Maeda, *J. Photochem. Photobiol., C*, 2011, **12**, 237–268.
16 J. Sato, N. Saito, H. Nishiyama and Y. Inoue, *Chem. Lett.*, 2001, **30**, 868–869.
17 A. Baszczuk, M. Jasiorski, M. Nyk, J. Hanuza, M. Mączka and W. Stręka, *J. Alloys Compd.*, 2005, **394**, 88–92.

18 X. Li, Z. Li and J. Yang, *Phys. Rev. Lett.*, 2014, **112**, 018301.
19 S. Tabata, N. Nishida, Y. Masaki and K. Tabata, *Catal. Lett.*, 1995, **34**, 245.
20 J. Sato, N. Saito, H. Nishiyama and Y. Inoue, *J. Phys. Chem. B*, 2001, **105**, 6061.
21 M. Guan, H. Zheng, L. F. Mei, M. S. Molokeev, J. Xie, T. Yang, X. W. Wu, S. F. Huang and Z. H. Huang, *J. Am. Ceram. Soc.*, 2015, **98**, 1182–1187.
22 F. S. Kao, *Mater. Chem. Phys.*, 2002, **76**, 295–298.
23 Y. P. Kang, B. Thuy, Y. Shimokawa, T. Hayakawa, S. Sakaida, L. Miao, S. Tanemura, S. Honda and Y. Iwamoto, *J. Lumin.*, 2016, **169**, 78–85.
24 M. Guan, H. Zheng, L. F. Mei, Z. H. Huang, T. Yang, M. H. Fang and Y. G. Liu, *Infrared Phys. Technol.*, 2014, **67**, 107–110.
25 X. M. Liu, C. K. Lin, Y. Luo and J. Lin, *J. Electrochem. Soc.*, 2007, **154**, J21–J27.
26 P. Li, Z. J. Wang, Z. P. Yang and Q. L. Guo, *J. Electrochem. Soc.*, 2011, **158**, H1201–H1205.
27 G. Kresse and J. Furthmüller, *Comput. Mater. Sci.*, 1996, **6**, 15–50.
28 P. E. Blöchl, *Phys. Rev. B: Condens. Matter Mater. Phys.*, 1994, **50**, 17953.
29 B. Hammer, L. B. Hansen and J. K. Nørskov, *Phys. Rev. B: Condens. Matter Mater. Phys.*, 1999, **59**, 7413.
30 J. A. Camargo-Martínez and R. Baquero, *Phys. Rev. B: Condens. Matter Mater. Phys.*, 2012, **86**, 195106.
31 S. E. Dali, V. S. Sundar, M. Jayachandran, M. Jayachandran and M. J. Chockalingam, *J. Mater. Sci. Lett.*, 1998, **17**, 619–623.
32 J. H. Edgar, *Properties of Group III Nitrides*, Institution of Electrical Engineers, 1994.
33 N. Fu, E. Li, Z. Cui, D. Ma, W. Wang, Y. L. Zhang, S. Song and J. Lin, *J. Alloys Compd.*, 2014, **596**, 92–97.
34 J. Black and P. Lublin, *J. Appl. Phys.*, 1964, **35**, 2462–2467.
35 D. C. Kim, D. L. Dheeraj, B. O. Fimland and H. Weman, *Appl. Phys. Lett.*, 2013, **102**, 142107.
36 S. Ves, U. Schwarz, N. E. Christensen, K. Syassen and M. Cardona, *Phys. Rev. B: Condens. Matter Mater. Phys.*, 1990, **42**, 9113.
37 D. Denzler, M. Olschewski and K. Sattler, *J. Appl. Phys.*, 1998, **84**, 2841–2845.
38 M. Muruganandham and Y. Kusumoto, *J. Phys. Chem. C*, 2009, **113**, 16144–16150.
39 I. Tsuji and A. Kudo, *J. Photochem. Photobiol., A*, 2003, **156**, 249–252.
40 H. J. Joyce, C. J. Docherty, Q. Gao, H. H. Tan, C. Jagadish, J. Lloyd-Hughes, L. M. Herz and M. B. Johnston, *Nanotechnology*, 2013, **24**, 214006.
41 V. R. Von Schenck and H. Muller-Buschbaum, *Z. Anorg. Allg. Chem.*, 1973, **398**, 24–30.
42 X. Y. Jiang, C. L. Yang, Y. X. Han, M. S. Wang and X. G. Ma, *Mater. Chem. Phys.*, 2016, **183**, 349–355.
43 H. C. Huang, C. L. Yang, M. S. Wang and X. G. Ma, *Renewable Energy*, 2018, **117**, 22–27.
44 F. Opoku, K. K. Govender, C. G. C. E. van Sittert and P. P. Govender, *ChemistrySelect*, 2017, **2**, 6304–6316.
45 J. Liu, X. B. Li, D. Wang, H. Liu, P. Peng and L. M. Liu, *J. Mater. Chem. A*, 2014, **2**, 6755–6761.
46 Y. Xu and M. A. A. Schoonen, *Am. Mineral.*, 2000, **85**, 543–556.
47 M. V. Putz, N. Russo and E. Sicilia, *Theor. Chem. Acc.*, 2005, **114**, 38–45.
48 Y. Xu and M. A. A. Schoonen, *Am. Mineral.*, 2000, **85**, 543–556.
49 H. C. Huang, C. L. Yang, M. S. Wang and X. G. Ma, *Sol. Energy Mater. Sol. Cells*, 2017, **170**, 233–238.
50 Y. M. Lin, Z. Y. Jiang, C. Y. Zhu, X. Y. Hu, H. Y. Zhu, X. D. Zhang, J. Fan and S. H. Lin, *Int. J. Hydrog. Energy*, 2013, **38**, 5209–5214.
51 S. B. Kokane, S. D. Sartale, C. A. Betty and R. Sasikala, *RSC Adv.*, 2014, **4**, 55539–55547.
52 M. Nolan and S. D. Elliott, *Phys. Chem. Chem. Phys.*, 2006, **8**, 5350–5358.
53 Q. Y. Xue, H. J. Liu, D. D. Fan, L. Cheng, B. Y. Zhao and J. Shi, *Phys. Chem. Chem. Phys.*, 2016, **18**, 17912–17916.
54 B. Radisavljevic, A. Radenovic, J. Brivio, V. Giacometti and A. Kis, *Nat. Nanotechnol.*, 2011, **6**, 147–150.
55 H. Zhang, L. Liu and Z. Zhou, *RSC Adv.*, 2012, **2**, 9224–9229.
56 F. Opoku, K. K. Govender, C. G. C. E. van Sittert and P. P. Govender, *Int. J. Quantum Chem.*, 2018, **118**, e25505.
57 F. Opoku, K. K. Govender, C. G. C. E. van Sittert and P. P. Govender, *New J. Chem.*, 2017, **41**, 11701–11713.